Check for updates

Batteries & Supercaps

Research Article
doi.org/10.1002/batt.202500263

Chemistry Europe
European Chemical Societies Publishing

www.batteries-supercaps.org

On the Mass Transport in Tubular Vanadium Redox Flow Batteries

Lotanna Onua, Alexandros Filipas, Thomas F. Fuller, and Nian Liu*

Efficient mass transport is critical for tubular flow battery performance and for its eventual scale-up; yet the influence of design parameters like electrode fiber filling density, internal membrane volume, and electrode structure remains largely unexplored. Herein, a tubular all-vanadium flow battery with a fibrous 4 mg cm^{-1} electrode filling density and a 0.238 cm internal diameter (ID) membrane is fed with dilute vanadium electrolyte at varying flow rates, and its mass transfer coefficient is calculated. The filling densities are increased to 8 and 16 mg cm^{-1}, where the 4 mg cm^{-1} shows the highest mass transfer coefficient, 2.64×10^{-6} cm s^{-1}. Decreasing the internal membrane diameter to 0.144 and 0.116 cm while restraining the 4 mg cm^{-1} filling density reveals the 0.238 cm diameter results in the largest mass transfer coefficient. Comparing a solid electrode to the 4 mg cm^{-1}, 0.238 cm ID electrode, the solid electrode reports the highest mass transfer coefficient, 2.56×10^{-5} cm s^{-1}. These findings surprisingly demonstrate that fibrous electrodes, despite their higher total surface area, do not inherently lead to improved mass transfer performance in tubular flow batteries, rather, it is the amount of available surface area and the uniformity in electrolyte flow, seen in the solid graphite electrode, that is critical for mass transfer.

1. Introduction

Reactant mass transport, within an electrochemical system, is the movement of active species from the bulk of electrolyte to the surface of an electrode where the charge transfer occurs;[1,2] this movement often dictates the overall rate of reaction of the system.[2] Electrochemical flow systems increase mass transport by introducing forced convection, which brings more reactants to the electrode surface by thinning the diffusion boundary layer (**Figure 1**a).[3] Redox flow batteries (RFBs) are a type of electrochemical flow system that store its electrolyte in external tanks then uses pumps to force the electrolyte to flow through its cell body.[4] The mass transport behavior of planar designs has been thoroughly investigated, and its conclusions have been used to optimize planar flow battery stacks for scale-up.[5,6]

Recently, tubular geometry (Figure 1b–f) has been reported for RFBs as a promising alternative to conventional planar batteries;[7–9] it is proposed that the increase in electrode surface area to volume ratio can improve the overall volumetric performance.[8,10] However, the effects of this tubular geometry have not been fully characterized. Prior research analytically modeled the impact of a tubular structure on the current distribution through various electrode materials for RFBs.[11] Still, the mass transport of tubular flow RFBs has yet to be thoroughly explored. This gap is especially important as researchers have recently demonstrated an all-vanadium tubular stack with a performance that rivals planar stacks.[12] With this manufacturing and performance milestone, it is essential for the tubular specific mass transport properties to be studied; this will provide crucial insights for future design optimization.

A common method for investigating mass transport in electrochemical systems are limiting current experiments. The limiting current is a point in which the current response no longer increases with increasing voltage.[13] This phenomenon occurs when there is a lack of reactants on the surface.[3] The current response then becomes dictated by the rate at which reactants can reach the electrode surface, thus becoming mass transfer limited.[14,15] Previous researchers have used limiting current experiments to derive mass transfer coefficients for planar flow batteries and fuels cells,[16–21] but those studies used customized planar flow fields, thus making their conclusions nongeneralizable toward tubular geometries. A select few have examined mass transfer in tubular electrochemical reactors, but a majority have been computational studies that used simplifying assumptions, thus not reflecting reality.[20,22,23] Some have conducted experiments, but complex woven felts or meshed electrode designs were used, which can convolute the transport phenomena by generating eddies.[24,25]

The aim of this study is to experimentally investigate the mass transport in a tubular all-vanadium battery using limiting current experiments. This study avoids convoluting the transport phenomena by employing smooth graphite rods and aligned carbon fibers (**Figure 2**a) as electrodes rather than complex graphite felts (Figure 2b). Three experimental parameters were investigated: electrode filling density, membrane internal diameter, and electrode structure. For the first parameter, the filling densities,

L. Onua, A. Filipas, T. F. Fuller, N. Liu
School of Chemical and Biomolecular Engineering
Georgia Institute of Technology
Atlanta, Georgia 30332, USA
E-mail: nian.liu@chbe.gatech.edu

Supporting information for this article is available on the WWW under https://doi.org/10.1002/batt.202500263

© 2025 The Author(s). Batteries & Supercaps published by Wiley-VCH GmbH. This is an open access article under the terms of the Creative Commons Attribution-NonCommercial License, which permits use, distribution and reproduction in any medium, provided the original work is properly cited and is not used for commercial purposes.

© 2025 The Author(s). Batteries & Supercaps published by Wiley-VCH GmbH

Research Article
doi.org/10.1002/batt.202500263
Chemistry Europe
European Chemical Societies Publishing

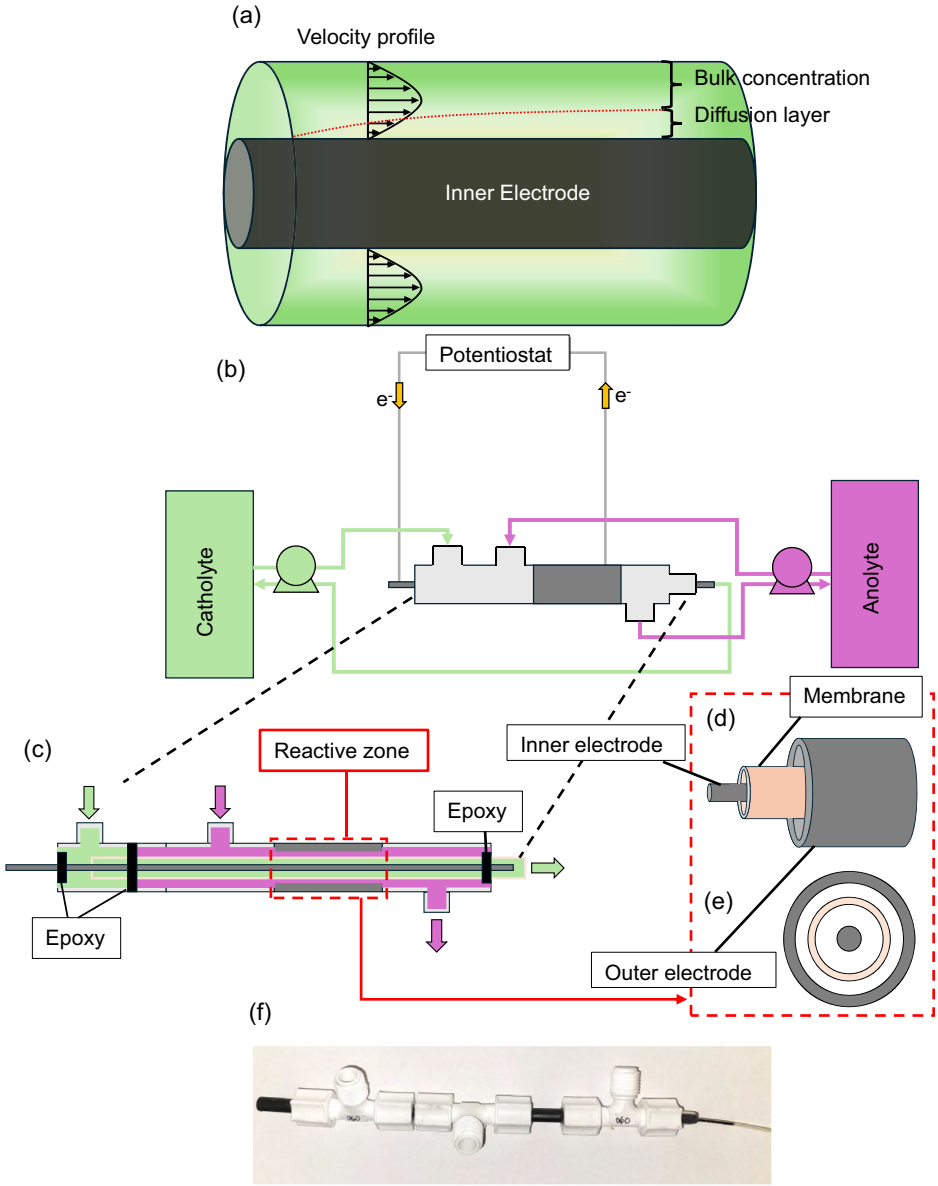

Figure 1. a) Schematic of fully developed electrolyte velocity profile and a growing concentration gradient surrounding the inner electrode. b) A schematic of a tubular flow battery. c) A cross-section schematic of a tubular flow battery. d) Side profile view of reactive zone. e) Front profile view of reactive zone. f) A tubular RFB constructed with tee fittings.

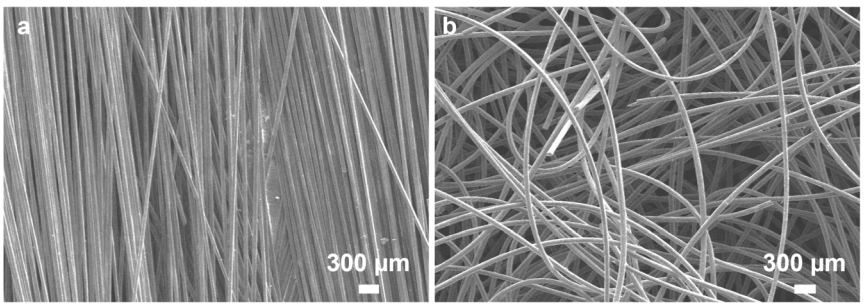

Figure 2. a) SEM image of aligned carbon fibers (7 µm ID) used as an electrode in this study. b) SEM image of typical graphite felt (12 µm ID) which can convolute mass transfer phenomena.

© 2025 The Author(s). Batteries & Supercaps published by Wiley-VCH GmbH

25666223, 0, Downloaded from https://chemistry-europe.onlinelibrary.wiley.com/doi/10.1002/batt.202500263 by University of Ulsan, Wiley Online Library on [11/11/2025]. See the Terms and Conditions (https://onlinelibrary.wiley.com/terms-and-conditions) on Wiley Online Library for rules of use; OA articles are governed by the applicable Creative Commons License

25666223, 0, Downloaded from https://chemistry-europe.onlinelibrary.wiley.com/doi/10.1002/batt.202500263 by University of Ulsan, Wiley Online Library on [11/11/2025]. See the Terms and Conditions (https://onlinelibrary.wiley.com/terms-and-conditions) on Wiley Online Library for rules of use; OA articles are governed by the applicable Creative Commons License

which is the mass of each electrode divided by their respective lengths, were 4, 8, and 16 mg cm^{-1}. For the second parameter, the internal membrane diameters were 0.116, 0.144, and 0.238 cm, and all electrodes had a constant filling density of 4 mg cm^{-1}. For the third parameter, two electrode structures were chosen: a solid graphite rod and a bundle of carbon fibers. The mass transfer coefficients were derived for each experimental setup, and generalizations of their effects were summarized.

2. Experimental Section

2.1. Electrode Pretreatment and Electrolyte Preparation

Pristine commercial PAN-based carbon fibers were purchased from Toray Composite Materials America. Pristine carbon fibers underwent thermal treatment. For the primary thermal treatment, the carbon fibers were heated in a tube furnace to 500 °C for 2 h, including a 1 h ramp-up, under argon gas. A 1.65 M total concentration of vanadium electrolyte, VO^{2+} and VO_2^+, at 50% state-of-charge (SOC) provided by Stryten Energy was diluted to 0.005 M VO^{2+} and 0.005 M VO_2^+ using 4 M of H_2SO_4.

2.2. Symmetric Cell Construction

All flow cells were assembled using a 20 cm tubular Nafion membrane (PermaPure). The internal diameter for the Section 3.2 experiments varied from 0.238, 0.144, and 0.116 cm. The inner electrode, graphite rod (Ohio Carbon Blank) or carbon fibers (24 and 20 cm, respectively), was inserted into the membrane. Three different filling densities were experimented with the carbon fiber electrodes: 4, 8, 16 mg cm^{-1}. The graphite rod had an outer diameter of 0.15 cm and a filling density of 32 mg cm^{-1}. ¼-inch plastic tee fittings (McMaster) and ¼-inch polypropylene plastic tubes (McMaster) were used as the cell casing and connectors (Figure 1f), respectively. For the reactive zone (Figure 1d,e), a 5 cm graphite tube (Ohio Carbon Blank) is placed between the inlet and outlet for the anolyte. Within the 5 cm length of the reactive zone, the graphite rod had a total surface area of 2.35 cm^{-2} while the graphite tube had an internal total surface area of 7.47 cm^{-2}.

2.3. Electrochemical Measurements

A symmetric cell test was conducted using two 500 mL beakers of the dilute vanadium, VO^{2+} and VO_2^+ at 50% SOC, as reservoirs. This experiment was conducted using dilute electrolyte for both the positive electrolyte and negative electrolyte to decrease the amount of vanadium ion crossover due to concentration differences across the membrane. To study the inner electrode (Figure 1c) at limiting currents, the electrolyte was pumped at volumetric flow rates incrementing from 1.2 to 13.1 mL min^{-1} using a peristaltic pump (MasterFlex) while the outer side of the membrane was held at a constant flow rate of 26.6 mL min^{-1}. This flow rate was found to be sufficiently high to isolate mass transfer effects from the counter electrode (graphite tube), as seen in (Figure S1, Supporting Information). The flow rate increments were the same for each configuration, thus changing the velocity at which the electrolyte flowed past the electrode surface. Polarization measurements were captured using an SP-200 potentiostat (Biologic). At each flow rate, the battery was polarized from 50 to 900 mV, with the voltage being applied for 20 s; its current responses were recorded. The limiting current was determined when the current increased below a threshold (0.025 mA). The utilization of the reactants was calculated to be below 5% for all cases.

2.4. Governing Equations

The hydraulic diameter, d_h, of the annular system is necessary for calculating important dimensionless numbers and mass transfer coefficients. The cross-sectional area of an individual fiber, A_{fiber}, was calculated in Equation (1) using d_f, which is the diameter of an individual fiber. Once the fibers are bundled into a respective filling density, they are treated as though they are one solid material. This approach is to calculate the cross-sectional area of the bundle. A_{bundle} is calculated using Equation (2). Equation (3) calculates the theoretical diameter of the solid bundle of carbon fibers, d_{bundle}. Finally, the hydraulic diameter is calculated where d_{m_i} is the inner diameter of the membrane. This derivation for the hydraulic diameter simplifies the complex, porous nature of these individual fibers as one solid bundle of fibers. It is assumed that because these fibers are laterally aligned, the total cross-sectional area of all of the fibers will not change based on individual fiber orientation.

$$A_{fiber} = \left(\frac{d_f}{2}\right)^2 \times \pi \tag{1}$$

$$A_{bundle} = A_{fiber} \times \#\,\text{of fibers} \tag{2}$$

$$d_{bundle} = 2 \times \sqrt{\frac{A_{bundle}}{\pi}} \tag{3}$$

$$d_h = d_{m_i} - d_{bundle} \tag{4}$$

The superficial velocity, $v_{superficial}$, which is the velocity through the membrane if there was no solid object obstructing flow, was determined by dividing the volumetric flow rate, Q, by the inner cross-sectional area of the membrane, A_{m_i}.

$$v_{superficial} = \frac{Q}{A_{m_i}} \tag{5}$$

For the fibrous bundle, the porosity, ϕ, was calculated by first determining the void area, A_{void}, in Equation (6).

$$A_{void} = \frac{\pi}{4}\left(d_{mi}^2 - d_f^2 \times \#\,\text{of fibers}\right) \tag{6}$$

The porosity was calculated by the following equation.

$$\phi = \frac{A_{void}}{A_{m_i}} \tag{7}$$

© 2025 The Author(s). Batteries & Supercaps published by Wiley-VCH GmbH

Research Article
doi.org/10.1002/batt.202500263
Chemistry Europe
European Chemical Societies Publishing

25666223, 0, Downloaded from https://chemistry-europe.onlinelibrary.wiley.com/doi/10.1002/batt.202500263 by University of Ulsan, Wiley Online Library on [11/11/2025]. See the Terms and Conditions (https://onlinelibrary.wiley.com/terms-and-conditions) on Wiley Online Library for rules of use; OA articles are governed by the applicable Creative Commons License

Finally, the pore-phase velocity, v_{pore}, which is the velocity of the electrolyte that travels through the pores of the fiber bundle, was determined by using the following equation.

$$v_{pore} = \frac{v_{superficial}}{\phi} \tag{8}$$

The Reynolds number is described below in Equation (9), where v is the kinematic viscosity of the electrolyte. To confirm fully developed flow was reached, the hydraulic length was calculated using the Reynolds number and hydraulic diameter in Equation (10). Even for the highest v_{pore}, the hydraulic length was less than 1 cm.

$$Re = \frac{v_{pore} d_h}{v} \tag{9}$$

$$L_h = 0.05 d_h Re \tag{10}$$

The mass transfer coefficient can be determined from the conservation of mass. To use that equation, the specific surface area, a, is first calculated using the volume of an individual fiber, V_f, where d_f is the diameter of the carbon fiber, L_r is the length of the reactive zone.

$$V_f = \frac{\pi d_f^2 L_r}{4} \tag{11}$$

$$a = \pi d_f L_r \times \frac{1-\phi}{V_f} \tag{12}$$

$$k_m a c_i = -v_{pore} \frac{dc_i}{dy} \tag{13}$$

The vanadium ion concentration of the outlet is calculated by integrating Equation (13), where c_i^{in} is the inlet electrolyte concentration, c_i^{out} is the outlet electrolyte concentration. Even though the utilization was calculated to be below 5%, the change in concentration was still accounted for.

$$c_i^{out} = c_i^{in} \exp\left(-\frac{k_m a L_r}{v_{pore}}\right) \tag{14}$$

The relation between the limiting current and the concentration where d_{mi} is the diameter of the membrane can be expressed.[21]

$$I_{lim} = nF\pi d_{m_i} L_r v_{pore} (c_i^{in} - c_i^{out}) \tag{15}$$

The mass transfer coefficient can further be calculated based on the limiting current and the physical features of the system.

$$k_m = -\frac{v_{pore}}{aL_r} \ln\left(1 - \frac{I_{lim}}{nF\pi d_{mi} L_r c_i^{in} v_{pore}}\right) \tag{16}$$

The dimensionless number, w, is calculated using the diffusivity coefficient, D.[26] When $w << 1$, the Levich approximation can be applied, which characterizes the diffusion boundary layer as being extremely thin.[13] This number is used to identify if an electrochemical flow system is convectively controlled.

$$w = \frac{L_r D}{v_{pore} d_h^2} \tag{17}$$

3. Results and Discussion

3.1. Varying Fibrous Electrode Filling Density

Three batteries of the same membrane internal diameter, 0.238 cm, were tested using three different filling densities of fibrous electrode: 4, 8, and 16 mg cm^{-1}. Scanning electron microscopy (SEM) and X-ray computed tomography (CT) cross-section images of each membrane with its respective electrode filling density were captured (**Figure 3**) to visualize the different void areas of each filling density within the membrane.

The three filling densities: 4, 8, and 16 mg cm^{-1} (**Figure 4**a–c) were polarized from 50 to 900 mV, but only its reduction of VO_2^+

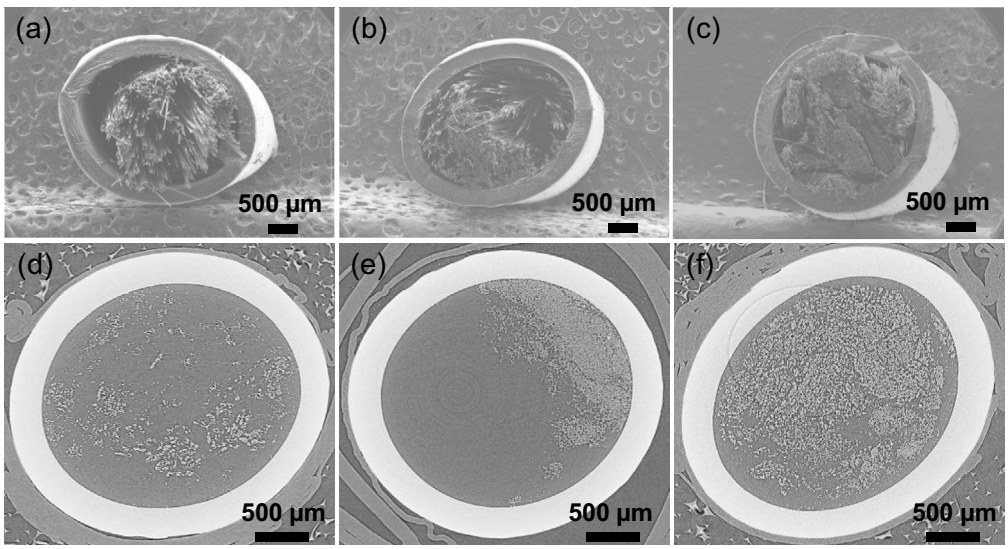

Figure 3. SEM images of fibrous electrode filling densities in 0.238 cm ID membranes. a) 4. b) 8. c) 16 mg cm^{-1}. X-ray CT scans of fibrous electrode filling densities in 0.238 cm ID membranes. d) 4. e) 8. f) 16 mg cm^{-1}.

© 2025 The Author(s). Batteries & Supercaps published by Wiley-VCH GmbH

Research Article
doi.org/10.1002/batt.202500263
Chemistry Europe
European Chemical Societies Publishing

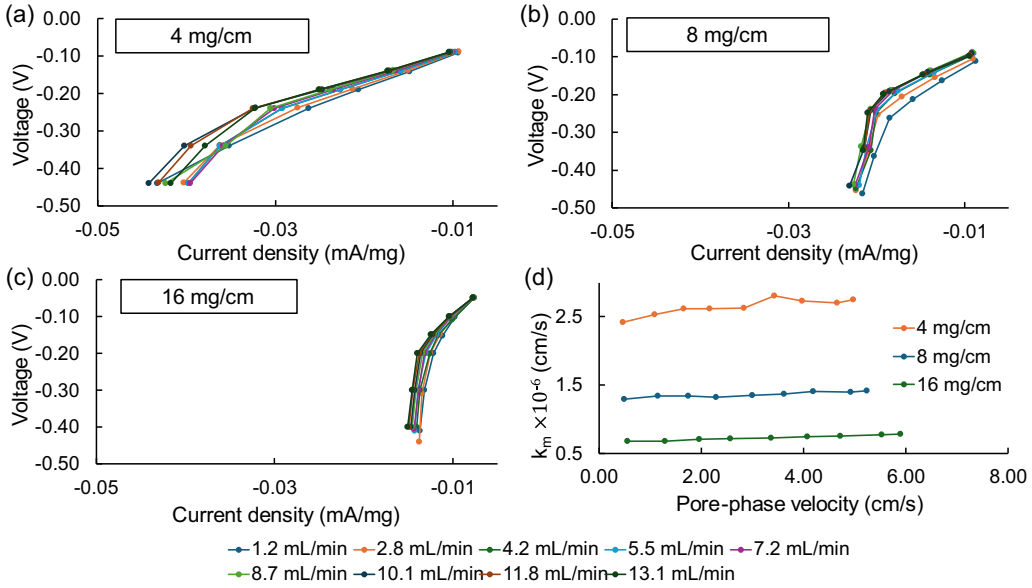

Figure 4. Normalized current responses of different fibrous filling densities. a) 4. b) 8. c) 16 mg cm^{-1}. d) Dependance of mass transfer coefficient on velocity for different filling densities.

to VO^{2+} is shown. The current response for the lowest flow rate, 1.2 mL min^{-1}, was recorded. Its change in current began to plateau around −0.5 V, indicating it had reached a limiting current. The subsequent flow rates, 2.8 through 13.1 mL min^{-1}, followed a similar pattern with each current response plateauing around −0.5 V. This experimental process was repeated for the 8 and 16 mg cm^{-1} filling densities (Figure 4b,c). For the 4 mg cm^{-1} filling density, the flow rate and by extension, the pore-phase velocity increased, but there was barely any change between the current responses for the lowest velocity and the highest velocity: 2.5 and 2.8 mA, respectively. Using Equation (16), the mass transfer coefficient was calculated and plotted against the pore-phase velocity (Figure 4d); the average mass transfer coefficient was 2.64×10^{-6} cm s^{-1}. This experimental coefficient is similar to simulated values from a previous tubular electrochemical study that modeled laminar flow; 4.51×10^{-6} and 3.24×10^{-6} cm s^{-1}.[26] Uniquely, its dependance on pore-phase velocity was determined to be $k_m \propto v^{0.055}$ which is extremely weak. This signals the mass transfer is significantly influenced by diffusion as opposed to convection.[27] The 8 and 16 mg cm^{-1} electrodes exhibited higher raw limiting currents than the 4 mg cm^{-1} electrode, averaging 2.8 and 3.0 mA (**Table 1**), respectively, compared to 2.7 mA. Contrarily, they both averaged lower mass transfer coefficients, 1.37×10^{-6} and 0.74×10^{-6} cm s^{-1}, and even weaker relationships with pore-phase velocity. This result can be explained by their normalized current responses (Figure 4b,c), where the 4 mg cm^{-1} has higher current densities than the 8 and 16 mg cm^{-1} electrodes, respectively. The normalized responses reveal underutilization of the total fibrous electrode surface. With a porous electrode, preferential flows and stagnant zones can become prominent. This can occur when a majority of the electrolyte preferentially flows through small channels within the bundled fibers, thus increasing its velocity, while a smaller portion of the electrolyte slowly flows through the rest of the volume, almost becoming stagnant.[27] This greatly reduces the surface area it contacts.[28] This phenomenon becomes more present at higher filling densities where the fibers are more compressed.[29–32] Because the 4 mg cm^{-1} electrode had the lowest filling density, and by extension, the least compression, more of its electrode surface area was utilized compared to the 8 and 16 mg cm^{-1} electrode. Additionally, the overall weak dependance on velocity is also a result of the presence of preferential flow and stagnant zones. Researchers have found that mass transport within flow systems that experience preferential flows and stagnant zones are dictated by molecular diffusion.[27] It is also due to the presence of preferential flow that Equation (17) is not applicable to this section. Because electrolyte preferentially flows through channels that

Table 1. Electrochemical performance of solid graphite electrode and the varying fibrous filling densities.

Electrode filling density [mg cm^{-1}]	Number of strands	Total surface area [cm^{-2}]	Hydraulic diameter [cm]	Average pore-phase velocity [cm s^{-1}]	Average experimental limiting current [mA]	Average experimental limiting current density [mA mg^{-1}]	Average $k_m \times 10^{-6}$ [cm s^{-1}]
Graphite (32)	–	2.35	0.0880	4.42	−3.20	−0.0199	29.5
4	≈5000	291.89	0.1848	2.80	−2.70	−0.136	2.64
8	≈10 000	584.10	0.1627	2.96	−2.80	−0.070	1.35
16	≈20 000	1168.20	0.1316	3.33	−3.00	−0.037	0.727

© 2025 The Author(s). Batteries & Supercaps published by Wiley-VCH GmbH

25666223, 0, Downloaded from https://chemistry-europe.onlinelibrary.wiley.com/doi/10.1002/batt.202500263 by University of Ulsan, Wiley Online Library on [11/11/2025]. See the Terms and Conditions (https://onlinelibrary.wiley.com/terms-and-conditions) on Wiley Online Library for rules of use; OA articles are governed by the applicable Creative Commons License

25666223, 0, Downloaded from https://chemistry-europe.onlinelibrary.wiley.com/doi/10.1002/batt.202500263 by University of Ulsan, Wiley Online Library on [11/11/2025]. See the Terms and Conditions (https://onlinelibrary.wiley.com/terms-and-conditions) on Wiley Online Library for rules of use; OA articles are governed by the applicable Creative Commons License

are much smaller in diameter than the actual membrane, and it is impossible to estimate those diameters, there is no way to accurately calculate Equation (17). Additionally, experimental visualization of preferential flow in reactor systems can be very difficult and is typically done using transparent materials and high-speed cameras to capture the flow of fluid.[33–35]

3.2. Varying Membrane Inner Diameter

The effect of membrane internal volume was investigated by maintaining the fibrous electrode filling density, 4 mg cm^{-1}, and varying the inner diameter of the membrane. Three different internal membrane diameters were experimented: 0.116, 0.144, and 0.238 cm. SEM and X-ray CT images of the different membrane diameters were captured (**Figure 5**) and the difference in cross-sectional void area was visualized.

Using the same filling density, 4 mg cm^{-1}, the internal diameter of the membrane varied from 0.238, 0.144, and 0.116 cm (**Figure 6**a–c) for each electrode configuration. Please note the 4 mg cm^{-1}, 0.238 cm ID electrode is the same electrode tested in Section 3.1. The electrodes were polarized from 50 to 900 mV, and its current responses recorded. The current density was normalized by the internal diameter of the membrane to isolate the effects of volume. The lowest flow rate's, 1.2 mL min^{-1}, current response consistently increased until it plateaued between −0.5 and −0.6 V for all the configurations, indicating the electrode at that specific flow rate has reached a limiting current. The subsequent flow rates, 2.8 through 13.1 mL min^{-1}, followed a similar pattern. For the 0.238 cm ID membrane, it averaged a raw current response of −2.70 mA (**Table 2**) and an average current density of −0.23 mA cm^{-3}. Its mass transfer coefficient was 2.64×10^{-6} cm s^{-1}. For the 0.144 ID and 0.116 cm ID, they averaged higher raw currents, −3.70 and −3.75 mA, as well as current densities, −0.421 and −0.543 mA cm^{-3}, respectively (Table 2). At first glance, these results seem to agree with existing literature on tubular reactors where maximizing the electrode surface area to volume ratio results in increased electrochemical performance,[36] but despite the higher currents, the 0.144 ID and 0.116 cm ID averaged lower mass transfer coefficients, 2.11×10^{-6} and 1.77×10^{-6} cm s^{-1}, respectively. This result is once again due to the compression of the fibers creating preferential flow, thus reducing the contact between the electrolyte and the electrode surface area. Figure 5 clearly shows the 0.238 cm ID has more cross-sectional void area compared to the 0.144 ID and 0.116 cm ID. These results agree with the previous section's results: more compression of the fibrous electrode limits the available surface area and leads to worst mass transfer performances. Similarly, the dimensionless number, *w*, cannot be accurately applied to this system due to the presence of preferential flows.

3.3. Solid Electrode versus Fibrous Electrode

A solid graphite rod electrode and the 4 mg cm^{-1} fibrous electrode, two extremes of the tubular RFB electrode structures, were tested and compared. The internal membrane diameter, 0.238 cm, was used for both electrodes. The graphite rod electrode, which has a filling density of 32 mg cm^{-1}, produced very low current responses when normalized by its mass in the reactive zone. Electrochemical impedance spectroscopy measurements (Figure S3, Supporting Information) for the graphite and fibrous electrodes were taken, and it was determined that the difference in electrical conductivity between the electrodes does not significantly affect the current response. This difference in current density can be attributed to the overall large difference in total surface area between the solid graphite rod and the 4 mg cm^{-1} fibrous electrode (Table 1). This trend sharply contrasts with the average mass transfer coefficients, where the graphite rod produced 2.95×10^{-5} cm s^{-1} (**Figure 7**b) compared to the 4 mg cm^{-1} electrode, 2.64×10^{-6} cm s^{-1} (Figure 5b). Additionally, the graphite rod electrode has a much stronger

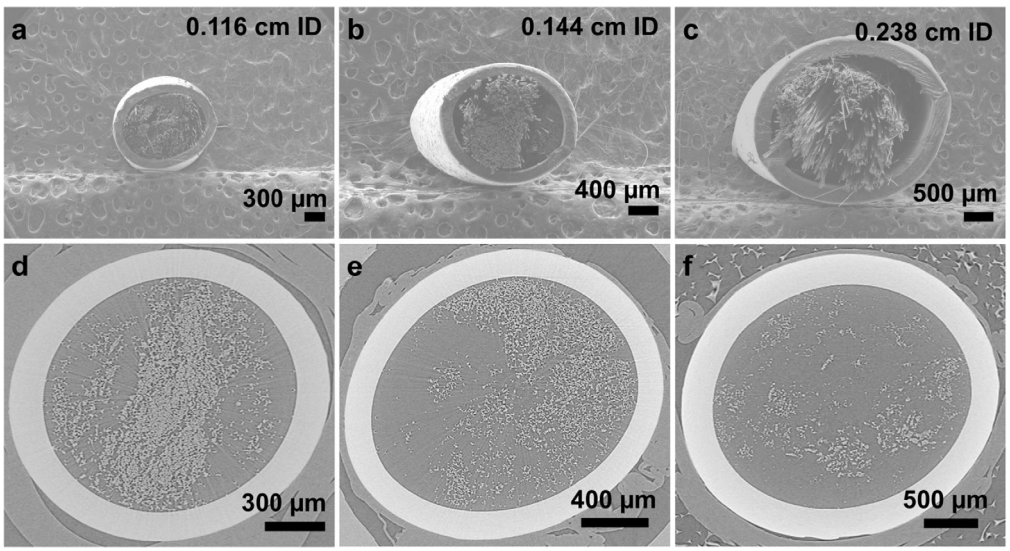

Figure 5. SEM image of 4 mg cm^{-1} carbon fiber inserted in membrane with various inner diameters. a) 0.116 ID. b) 0.144 ID. c) 0.238 cm ID. Cross-sectional X-ray CT scans of 4 mg cm^{-1} carbon fiber inserted in membrane. d) 0.116 ID. e) 0.144 ID. f) 0.238 cm ID.

© 2025 The Author(s). Batteries & Supercaps published by Wiley-VCH GmbH

Research Article
doi.org/10.1002/batt.202500263
Chemistry Europe
European Chemical Societies Publishing

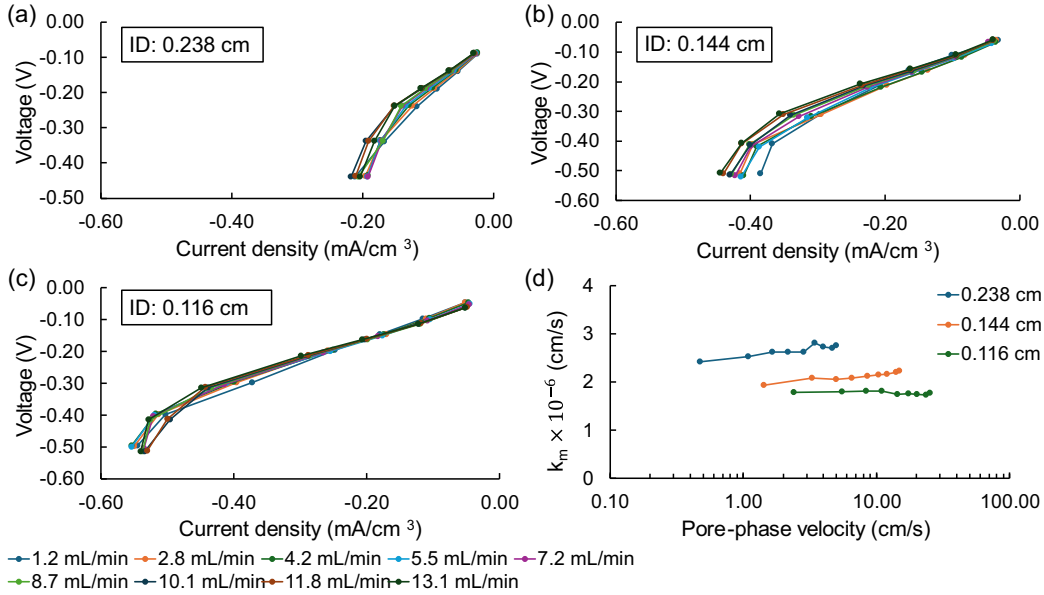

Figure 6. Normalized current responses of varying inner diameter with a constant filling density, 4 mg cm^{-1}. a) 0.238 ID. b) 0.144 ID. c) 0.116 cm ID. d) Mass transfer coefficients of 0.116, 0.144, and 0.238 cm ID membrane.

Table 2. Electrochemical properties with varying internal membrane diameter and a constant filling density, 4 mg cm^{-1}.

Membrane Internal Diameter [cm]	Total membrane volume [cm^{-3}]	Hydraulic diameter [cm]	Average Pore-phase velocity [cm s^{-1}]	Average Experimental limiting current [mA]	Average Experimental limiting current density [mA cm^{-3}]	Average $k_m \times 10^{-6}$ [cm s^{-1}]
0.116	6.908	0.0628	14.2	−3.75	−0.543	1.77
0.144	8.792	0.0908	8.44	−3.70	−0.421	2.11
0.238	14.444	0.1848	2.80	−2.70	−0.23	2.64

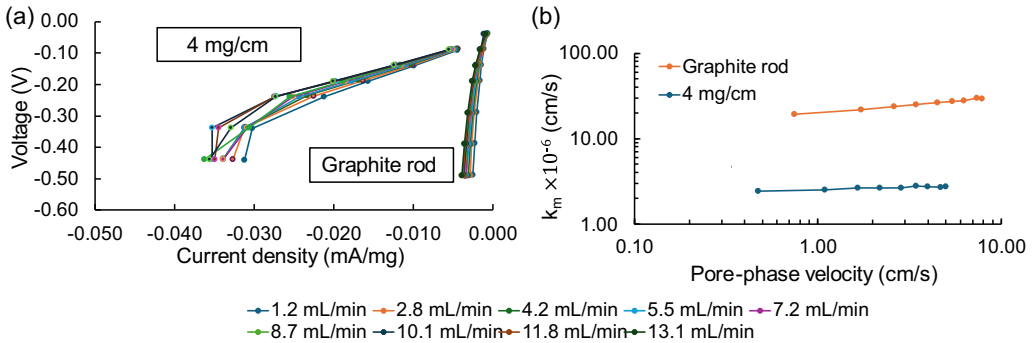

Figure 7. Normalized current responses of solid electrode and fibrous electrode. a) Graphite rod (32 mg cm^{-1}) and 4 mg cm^{-1} fiber electrode. b) Dependance of mass transfer coefficient on velocity for solid and fibrous electrode.

dependance of mass transfer coefficient on velocity with a relationship of $k_m \propto v^{0.18}$ compared to the $k_m \propto v^{0.055}$ relationship for the 4 mg cm^{-1} electrode. Due to its smooth, nontortuous surface, the electrolyte flows more uniformly around the surface of the electrode, thus inhibiting channeling. Although its average pore-phase velocity is not as fast as the smaller diameter membranes, 0.116 ID and 0.144 cm ID, the electrolyte gets to flow more uniformly around the surface of the electrode, thus completely utilizing its surface. This uniformity of electrolyte flow allows the influence of convection to be more prominent, thus increasing the mass transfer coefficient and the dependance on velocity. This aligns with earlier findings: maximizing accessible electrode surface area yields higher mass transport performance. The dimensionless number, w, was calculated for each flow rate for the graphite rod (**Figure 8**) against its limiting current. The data falls between the Levich approximation, which is when $w << 1$, thus indicating the diffusion boundary layer is extremely thin and transport is dictated by convection.[13,37]

© 2025 The Author(s). Batteries & Supercaps published by Wiley-VCH GmbH

25666223, 0, Downloaded from https://chemistry-europe.onlinelibrary.wiley.com/doi/10.1002/batt.202500263 by University of Ulsan, Wiley Online Library on [11/11/2025]. See the Terms and Conditions (https://onlinelibrary.wiley.com/terms-and-conditions) on Wiley Online Library for rules of use; OA articles are governed by the applicable Creative Commons License

Research Article
doi.org/10.1002/batt.202500263
Chemistry Europe
European Chemical Societies Publishing

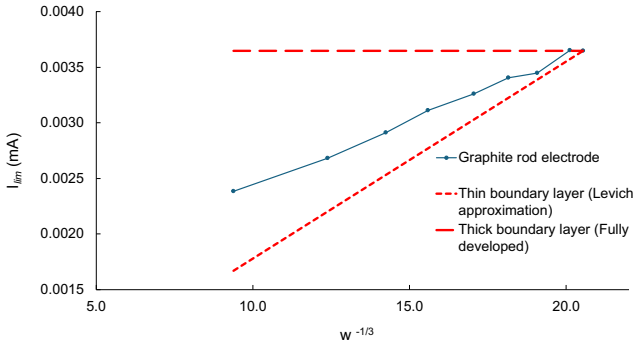

Figure 8. Limiting current for graphite rod electrode as a function of $w^{-1/3}$. The theoretical behavior is graphed for a thin boundary layer and a fully developed boundary layer.

When $w > 1$, the diffusion boundary layer is assumed to be much thicker or fully developed, thus making mass transport dictated by diffusion. For this system, the actual data falls between the two extremes. This explains why the graphite rod's mass transfer coefficient has a much stronger relationship with velocity, $k_m \propto v^{0.18}$, compared to the diffusion-controlled 4 mg cm^{-1} fibrous electrode, $k_m \propto v^{0.055}$. Convection has a stronger influence on the graphite rod electrode compared to the fibrous electrode.

The maximum volumetric and areal power densities were determined for each electrode configuration by calculating the total surface area of the individual fibers and the total volume the bundled fibers occupied. Both power densities used the voltage and current response from the highest flow rate, 13.1 mL min^{-1}, and were compared as seen in (**Figure 9**). The graphite electrode produced a significantly larger areal power density compared to all the fibrous electrodes, but its volumetric power density was extremely low. Interestingly, the fibrous electrodes all followed the same trend of the normalized current responses seen in the earlier sections. The 16 mg cm^{-1}, 0.238 cm ID electrode had the worst volumetric and areal performance overall, while the smaller diameter membranes produced significantly higher volumetric power densities. In applications where there is demand for high power and there are no size or cost restraints, the superior mass transfer of the solid graphite rod electrode coupled with its high areal power density makes it the preferred electrode configuration.

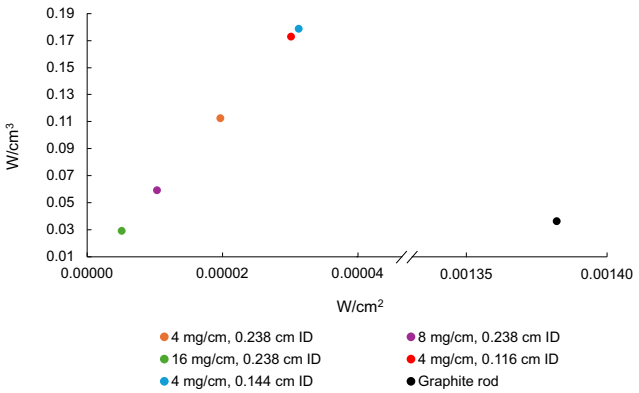

Figure 9. Comparison of maximum volumetric and areal power densities for each electrode configuration.

4. Conclusions

In this study, the parameters: electrode filling density, internal membrane diameter, and electrode structure were investigated. It was found that increasing the fibrous electrode filling density produced higher raw current responses, but when normalized by its own mass, it revealed reactive surface area underutilization issues with the lowest filling density, 4 mg cm^{-1}, producing the highest average mass transfer coefficient, of 2.64×10^{-6} cm s^{-1}. Additionally, larger internal membrane diameters produced larger mass transfer coefficients. Lastly, using a solid material as the electrode demonstrated a significant impact on performance by increasing the average mass transport coefficient, 2.95×10^{-5} cm s^{-1}, and its dependance on velocity, $k_m \propto v^{0.18}$, thus increasing the influence of convection compared to diffusive transport. Comparison of the volumetric and areal power densities found that the graphite rod had a significantly higher areal power density but an extremely low volumetric power density. Additionally, all the fibrous electrode configurations yielded low areal power densities, but their volumetric power densities increased with decreasing membrane internal volume. These findings overall revealed that preferential flow is a limiting factor for fibrous electrodes in tubular RFBs with respect to mass transport performance. These conclusions can be applied to future work on scaling up tubular reactors and optimizing their designs.

Acknowledgements

This work was partially supported by Stryten Energy. Additionally, this work was performed in part at the Georgia Tech Institute for Matter and Systems, a member of the National Nanotechnology Coordinated Infrastructure (NNCI), which is supported by the National Science Foundation (ECCS-2025462). The authors would like to thank Dr. Brian Berland at Stryten Energy for helpful discussion and Laxminarayanan Krishnan and Naeemah Alam for their contributions to CT imaging.

Conflict of Interest

The authors declare no conflict of interest.

Author Contributions

Lotanna Onua: conceptualization (lead); data curation (lead); formal analysis (lead); investigation (lead); methodology (lead); validation (lead); visualization (lead); writing—original draft (lead); writing—review and editing (lead). **Alexandros Filippas**: conceptualization (supporting); writing—review and editing (supporting). **Thomas F. Fuller**: formal analysis (supporting); writing—review and editing (supporting). **Nian Liu**: methodology (supporting); visualization (supporting); writing—review and editing (supporting).

© 2025 The Author(s). Batteries & Supercaps published by Wiley-VCH GmbH

25666223, 0, Downloaded from https://chemistry-europe.onlinelibrary.wiley.com/doi/10.1002/batt.202500263 by University of Ulsan, Wiley Online Library on [11/11/2025]. See the Terms and Conditions (https://onlinelibrary.wiley.com/terms-and-conditions) on Wiley Online Library for rules of use; OA articles are governed by the applicable Creative Commons License

Data Availability Statement

The data that support the findings of this study are available from the corresponding author upon reasonable request.

Keywords: all-vanadium redox flow batteries · carbon fibers · diffusion layer · limiting current density · membrane diameters · tubular electrochemical reactors

[1] J. B. Flanagan, L. Marcoux, *J. Phys. Chem.* **1974**, *78*, 718.
[2] M. Thompson, O. V. Klymenko, R. G. Compton, *J. Electroanal. Chem.* **2005**, *575*, 329.
[3] N. Ibl, O. Dossenbach, *Convective Mass Transport*, Springer Science, New York **1983**.
[4] R. M. Darling, K. G. Gallagher, J. A. Kowalski, S. Ha, F. R. Brushett, *Energy Environ. Sci.* **2014**, *7*, 3459.
[5] H. Zhang, W. Lu, X. Li, *Electrochem. Energy Rev.* **2019**, *2*, 492.
[6] B. Jung, S. Park, C. Lim, W. H. Lee, Y. Lim, J. Na, C.-J. Lee, H.-S. Oh, U. Lee, *Chem. Eng. J.* **2021**, *424*, 130265.
[7] S. Ressel, A. Laube, S. Fischer, A. Chica, T. Flower, T. Struckmann, *J. Power Sources* **2017**, *355*, 199.
[8] S. Ressel, P. Kuhn, S. Fischer, M. Jeske, T. Struckmann, *J. Power Sources Adv.* **2021**, *12*, 100077.
[9] Y. Wu, F. Zhang, T. Wang, P.-W. Huang, A. Filippas, H. Yang, Y. Huang, C. Wang, H. Liu, X. Xie, R. P. Lively, N. Liu, *Proc. Natl. Acad. Sci.* **2023**, *120*, e2213528120.
[10] C. Stolze, T. Janoschka, J. Winsberg, M. Strumpf, M. D. Hager, U. S. Schubert, *Energy Technol.* **2018**, *6*, 2296.
[11] A. Filippas, T. F. Fuller, N. Liu, *J. Electrochem. Soc.* **2024**, *171*, 093509.
[12] F. Brandes, S. Ressel, P. Kuhn, A. Laube, J. Ramthun, N. Janshen, A. Chica, C. Weidlich, M. Jeske, S. Fischer, T. Struckmann, *J. Power Sources* **2025**, *628*, 235839.
[13] Y. Wu, Z. Wang, *Electrochim. Acta* **1999**, *44*, 2281.
[14] F. C. Walsh, C. Ponce de León, *Electrochim. Acta* **2018**, *280*, 121.
[15] S. C. Perry, C. P. de León, F. C. Walsh, *J. Electrochem. Soc.* **2020**, *167*, 155525.
[16] O. M. Cornejo, I. Sirés, J. L. Nava, *Chem. Eng. J.* **2023**, *455*, 140603.
[17] S. Kumar, S. Jayanti, *J. Power Sources* **2016**, *307*, 782.
[18] L. F. Arenas, C. P. de León, F. C. Walsh, *Electrochim. Acta* **2016**, *221*, 154.
[19] A. A. Abahussain, C. P. de Leon, F. C. Walsh, *J. Electrochem. Soc.* **2018**, *165*, F198.
[20] J. Wang, T. Li, M. Zhou, X. Li, J. Yu, *Electrochim. Acta* **2015**, *173*, 698.
[21] X. You, Q. Ye, P. Cheng, *J. Electrochem. Soc.* **2017**, *164*, E3386.
[22] D. S. Ibrahim, C. Veerabahu, R. Palani, S. Devi, N. Balasubramanian, *Comput. Fluids* **2013**, *73*, 97.
[23] A. N. Colli, J. M. Bisang, *J. Electrochem. Soc.* **2018**, *165*, E81.
[24] J. Su, H.-Y. Lu, H. Xu, J.-R. Sun, J.-L. Han, H.-B. Lin, *Russ. J. Electrochem.* **2011**, *47*, 1293.
[25] K. Percin, O. Zoellner, D. Rall, M. Wessling, *ChemElectroChem* **2020**, *7*, 2665.
[26] B. K. Körbahti, *J. Electrochem. Soc.* **2014**, *161*, E3225.
[27] J. A. Moulijn, M. Makkee, R. J. Berger, *Catal. Today* **2016**, *259*, 354.
[28] J. Radolinski, H. Le, S. S. Hilaire, K. Xia, D. Scott, R. D. Stewart, *Sci. Rep.* **2022**, *12*, 4261.
[29] R. Jervis, M. D. R. Kok, T. P. Neville, Q. Meyer, L. D. Brown, F. Iacoviello, J. T. Gostick, D. J. L. Brett, P. R. Shearing, *J. Energy Chem.* **2018**, *27*, 1353.
[30] R. Banerjee, N. Bevilacqua, A. Mohseninia, B. Wiedemann, F. Wilhelm, J. Scholta, R. Zeis, *J. Energy Storage* **2019**, *26*, 100997.
[31] R. Gundlapalli, S. Jayanti, *J. Power Sources* **2019**, *427*, 231.
[32] J. Charvát, P. Mazúr, J. Dundálek, J. Pocedič, J. Vrána, J. Mrlík, J. Kosek, S. Dinter, *J. Energy Storage* **2020**, *30*, 101468.
[33] J. Fu, Y. Xiao, Z. Wang, Z. Cao, H. Gu, *Ann. Nucl. Energy* **2025**, *216*, 111287.
[34] Y. A. Hassan, E. E. Dominguez-Ontiveros, *Nucl. Eng. Des.* **2008**, *238*, 3080.
[35] U. M. López-García, P. E. Hidalgo, J. C. Olvera, F. Castañeda, H. Ruiz, G. Orozco, *Fuel* **2013**, *110*, 162.
[36] A. K. Ray, *Chem. Eng. Sci.* **1999**, *54*, 3113.
[37] V. G. Levich, *Physiochemical Hydrodynamics*, Prentice-Hall, Englewood Cliffs, NJ **1962**.

Manuscript received: April 7, 2025
Revised manuscript received: May 20, 2025
Version of record online:

© 2025 The Author(s). Batteries & Supercaps published by Wiley-VCH GmbH

25666223, 0, Downloaded from https://chemistry-europe.onlinelibrary.wiley.com/doi/10.1002/batt.202500263 by University of Ulsan, Wiley Online Library on [11/11/2025]. See the Terms and Conditions (https://onlinelibrary.wiley.com/terms-and-conditions) on Wiley Online Library for rules of use; OA articles are governed by the applicable Creative Commons License